Concentration profiles across twin boundaries in $YBa_2Cu_3O_{6+\delta}$

Qiu-Hong Hu, Krystyna Stiller, Eva Olsson, and Hans-Olof Andrén
Department of Physics, Chalmers University of Technology and University of Göteborg, S-412 96 Göteborg, Sweden

Pedro Berastegui and Lars-Gunnar Johansson
Department of Inorganic Chemistry, Chalmers University of Technology and University of Göteborg, S-412 96 Göteborg, Sweden

(Received 18 July 1997)

Twin boundaries in polycrystalline $YBa_2Cu_3O_{6+\delta}$ have been studied by atom-probe field-ion microscopy. Oxygen depletion at a twin boundary in a $\delta=0.6$ material was observed. The width of the depleted region was 6–7 nm. It agrees well with the width of oxygen depletion calculated from the oxygen-depleted twin boundary model by Jou and Washburn. However, a twin boundary in a $\delta=0.9$ material did not show any oxygen depletion. This study provides direct evidence of oxygen depletion at twin boundaries in polycrystalline $YBa_2Cu_3O_{6+\delta}$ ceramics. [S0163-1829(97)07541-3]

I. INTRODUCTION

Defects play a very important role in $YBa_2Cu_3O_{6+\delta}$ both in production and application of the material. The principal defects found in the materials are grain boundaries, twin boundaries, vacancies, and inclusions. These defects can be classified as interconnected defects and isolated defects depending on the way they arrange themselves. Grain boundaries and twin boundaries are usually interconnected defects in nature, vacancies and inclusions are isolated defects. The presence of defects decreases the superconducting volume, but apart from that, the defects play a rather different role in the transport of the supercurrent. Interconnected defects, particularly high-angle grain boundaries, limit the transport critical current density J_c. Isolated defects, on the other hand, may act as pinning centers to enhance the J_c. In applications where a high critical current is needed, it is highly desirable to eliminate the interconnected defects and to introduce proper isolated defects. The amount of high-angle grain boundaries can be decreased to a great extent by texturing the material. But, twin boundaries always exist as long as the structure is orthorhombic, since upon cooling below about 700 °C, $YBa_2Cu_3O_{6+\delta}$ undergoes a tetragonal-to-orthorhombic (T-O) phase transition, unless precautions are taken in the material processing. The orthorhombic phase is characterized by extensive twinning on {110} planes. The twin boundaries are therefore the most common interconnected defect in $YBa_2Cu_3O_{6+\delta}$ ceramics. In $YBa_2Cu_3O_{6+\delta}$ thin films for devices based on Josephson effects, where naturally occurring grain boundaries are avoided and artificial grain boundaries are introduced, twin boundaries become the dominant interconnected defect.

Theoretical investigations of the effects of twin boundaries on the superconducting order parameter and on flux motion have raised interesting questions, such as whether twin boundaries suppress the order parameter or enhance it.[1,2] Experimental investigations of the effects of twin boundaries on flux motion have provided many interesting results which showed a detailed dependence of the pinning strength on temperature, magnetic field, and the relative orientation between magnetic field, twin boundary plane, and the direction of transport current.[3–7]

In order to obtain a complete structural picture of twin boundaries, and establish the relation between twin boundary structure and the superconducting properties, structural features on a length scale corresponding to the coherence length, along the boundaries and across the boundaries need to be identified. However, the coherence length of the materials is very short, of the order of a nanometer and the coherence length in the a-b plane is 1.6–3 nm.[8,9] Therefore, for structural characterization of the twin boundaries, microscopy and microanalytical techniques with a spatial resolution in the order of a nanometer are highly desirable. In addition, the oxygen content is directly related to the concentration of a charge carrier in the materials. The carrier concentration at the twin boundary region is certainly a crucial factor determining the transport of the supercurrent across the twin boundaries. Hence, besides the high resolution, a high accuracy in the determination of oxygen concentration is equally desirable. Furthermore, one of the important features of defects is a strong dependence of the thermal history of the material. This requires that an ideal characterization of the twin boundary structure and properties should be made on the same sample with well-specified heat treatment and well-defined oxygen content.

Great effort has been made in transmission electron microscopy (TEM) of twin boundaries.[10] Only in very limited cases, field-ion microscopy (FIM) observations of twin boundaries were reported.[11–13] In this paper we present a study of twin boundaries in $YBa_2Cu_3O_{6+\delta}$ by atom-probe field-ion microscopy (APFIM),[14,15] which provides direct evidence of oxygen depletion at twin boundaries in an oxygen-deficient polycrystalline material.

II. EXPERIMENTAL DETAILS

The $YBa_2Cu_3O_{6+\delta}$ materials used were polycrystalline ceramics. The ceramics were prepared in the form of a pellet by solid-state sintering at temperatures of 970 to 990 °C for over 80 h in a flow of oxygen at atmospheric pressure.[16] After cooling from the sintering temperatures, fully oxygenated samples with $\delta=0.9$ were prepared by *in situ* annealing

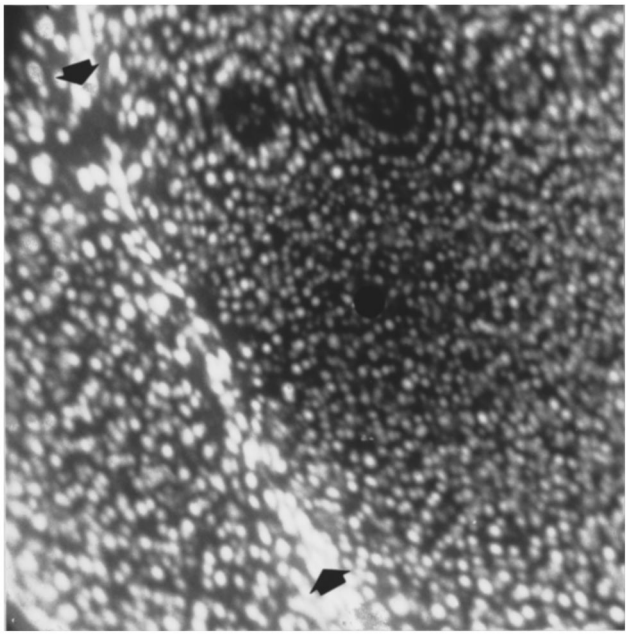

FIG. 1. FIM micrograph of a $YBa_2Cu_3O_{6.9}$ tip with a twin boundary indicated by arrows.

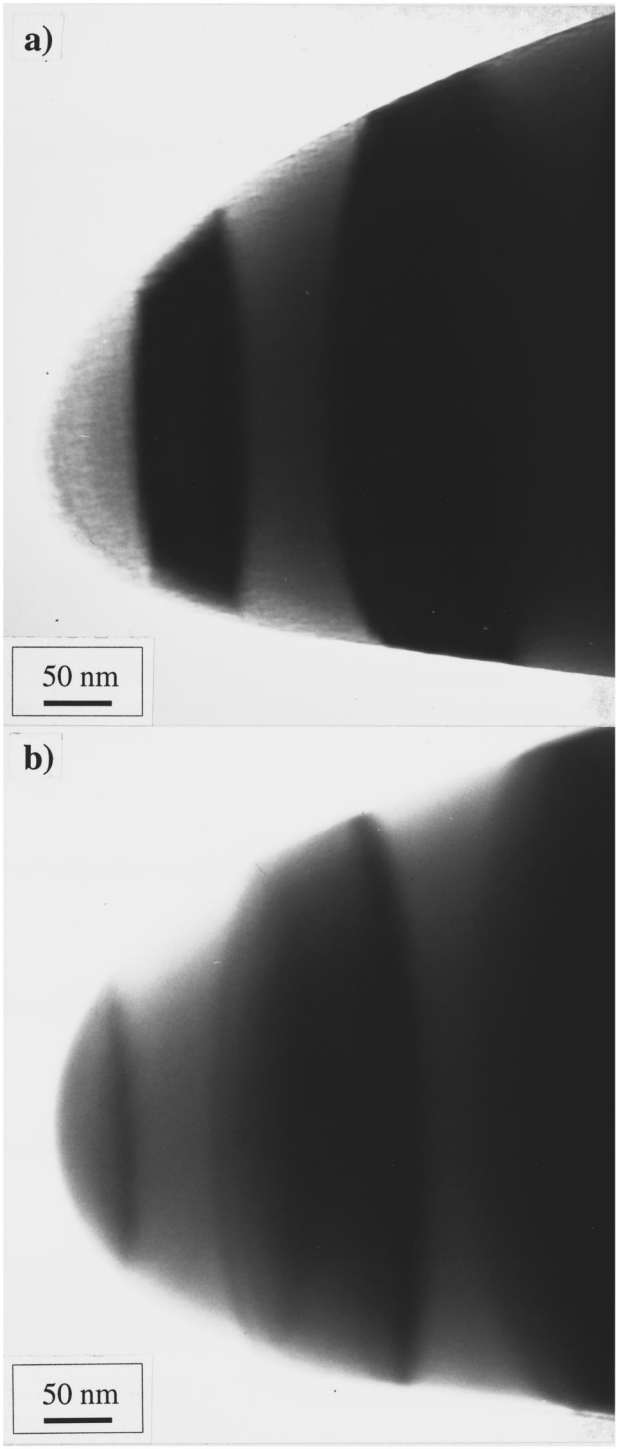

FIG. 2. Bright field transmission electron micrographs of a $YBa_2Cu_3O_{6.9}$ specimen before (a) and after (b) atom-probe analysis. It is evident that the twin boundary closest to the tip apex in (a) has been analyzed.

at 400 °C for 48 h in a flow of oxygen at atmospheric pressure and subsequent cooling to room temperature. Oxygen-deficient samples were prepared by the same annealing procedure in a flow of nitrogen at atmospheric pressure for varied annealing times. X-ray diffraction of the pellets was performed to detect any impurity phases, and to determine the lattice parameters. The relation between lattice parameters and oxygen content established by neutron diffraction and iodometric titration[17] was used to derive the oxygen content of the materials. The pellets were cut into pins with dimensions of about $0.3\times0.3\times10\,mm^3$ using a low speed diamond saw. Needle-shaped APFIM specimens were prepared by electropolishing.[18]

Each needle was examined in the transmission electron microscope to select those needles where a twin boundary was close enough to the tip apex to be analyzed by APFIM. The crystallographic orientation of the tip axis was determined from electron-diffraction patterns of the tip. The total length of the analyzed volume was determined by comparing TEM micrographs of the same tip before and after APFIM analysis. The comparison provided evidence that the boundary was within the analyzed length. FIM of the tip was performed to position the analyzing aperture at the center of the field ion image, so that the analyzed direction was coincident with the direction of the tip axis. This made it certain that the aperture was aimed on the twin boundary plane. TEM and FIM thus provided evidence that the twin boundary had been analyzed.

APFIM was performed in an energy-compensated atom-probe field-ion microscope.[19] The atom-probe analysis was performed at a specimen temperature of 80 K with a pulse fraction of 15% of the dc voltage and pulse frequency of 182 Hz.[20] The pressure in the vacuum chamber during all the analyses was about 30 nPa. Under such conditions, a systematic deficiency of oxygen was found to be below 2 at. % in the worst case.[21] FIM was performed at a specimen temperature of 80 or 90 K with N_2 as the imaging gas.

During atom-probe analysis surface atoms are ionized and removed from the needle-shaped specimen tip by field evaporation. Among these ions only those coming from within a circle of diameter of about 1–5 nm on the tip surface enter the mass spectrometer and may be chemically

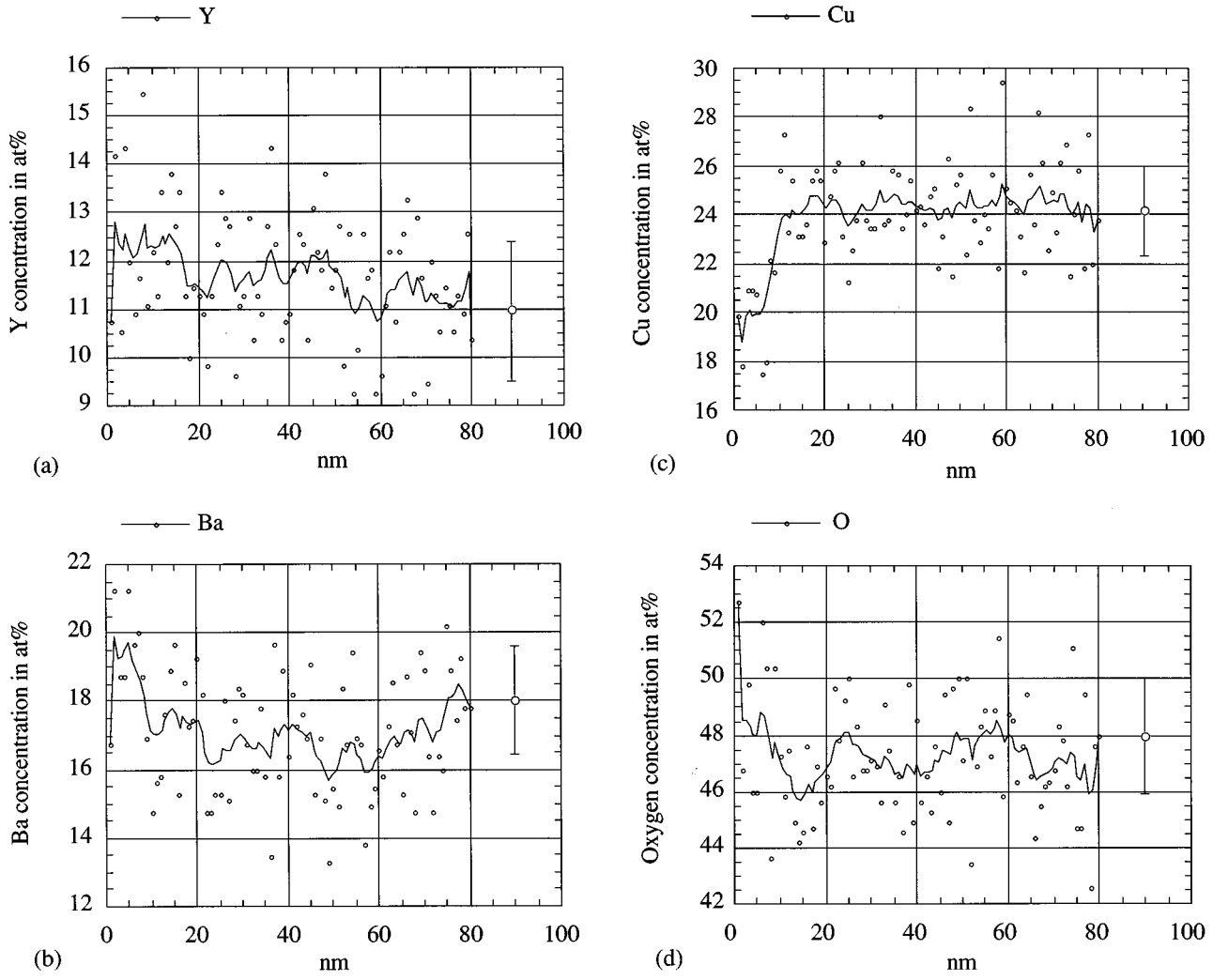

FIG. 3. Concentration profiles of Y (a), Ba (b), Cu (c), and O (d) in a $YBa_2Cu_3O_{6.9}$ specimen, with group size of 550 and average group length 1 nm. The curves are the smoothened curves (running mean over 3 blocks). Circles are measured data points. Error bars represent values of 2σ.

identified. In addition, the sequence of arrival of those ions at the detector is registered. As the analysis proceeds, atoms from a cylinder of about 1–5 nm in diameter and up to about 100 nm in length are collected. For the purpose of examining the concentration variation of the elements, concentration profiles are constructed by first dividing the whole detection sequence into groups of atoms. Each group, called a block, contains an equal number of atoms. The number of atoms in a block is referred to as the block sizes, and the corresponding length in the specimen (in nanometers) is called the block length. The variation in composition along the analyzed direction can therefore be obtained from the composition calculated for each block (see Ref. 15, pp. 29–31).

III. RESULTS

A field-ion micrograph of $YBa_2Cu_3O_{6.9}$ is shown in Fig. 1. The concentric rings represent consecutive atomic planes. It was established from TEM that an arrowhead bright band corresponds to a twin boundary. Unfortunately, in this case it was not possible to tilt the specimen so far that the boundary could reach the probe hole and atom-probe analysis of this boundary could not be made.

However, atom-probe analyses of twin boundaries in two other specimens were successful. In these cases the twin boundaries lay approximately perpendicular to the analyzed direction. Figure 2 shows a $YBa_2Cu_3O_{6.9}$ specimen before and after atom-probe analysis, Figs. 2(a) and 2(b), respectively. It is evident that the twin boundary closest to the tip apex in Fig. 2(a) has been analyzed. However, the composition profiles of this sample did not show any variation that could be connected to a boundary, Fig. 3.

TEM micrographs of a $YBa_2Cu_3O_{6.6}$ specimen before and after APFIM analysis are shown in Figs. 4(a) and 4(b). Since the probe aperture was at the center of the FIM images, its position on the tip surface should be at the place where local radius of the curvature of the tip profile was minimum in the TEM micrographs shown in Figs. 4(a) and 4(b). From Figs.

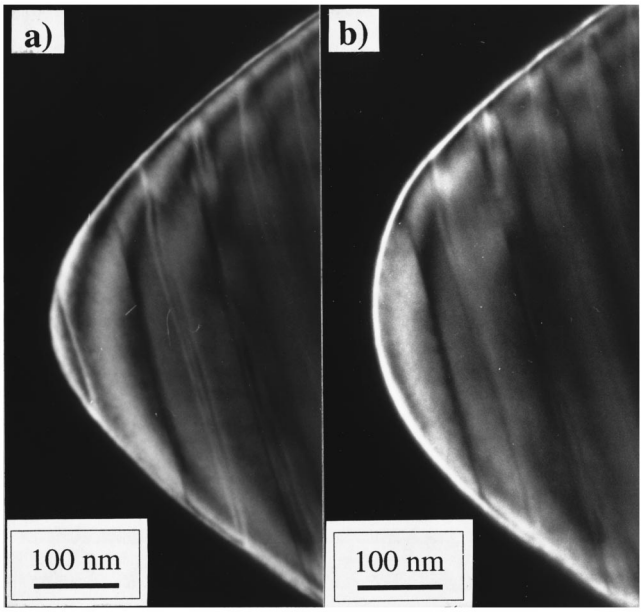

FIG. 4. Dark field transmission electron micrographs of a $YBa_2Cu_3O_{6.6}$ specimen before (a) and after (b) atom-probe analysis.

4(a) and 4(b) the analyzed direction was determined as 20° from the ⟨110⟩ direction. However, this orientation relation was insufficient to determine the crystallographic orientation of the analysis direction. By tilting the specimen 20°, another orientation of the tip was obtained, Fig. 5. In this orientation, the electron-diffraction pattern is a ⟨001⟩ pattern, and the tip axis was perpendicular to the (110) twin plane. From these pieces of information, we could conclude that the analyzed direction lay on the (-110) plane, 20° tilting up from the basal plane, Fig. 6.

In this analysis a total of 15 139 atoms were collected. The length of the analyzed volume was 42 nm as measured by comparing the two micrographs in Fig. 4. From these two numbers, we can get the average number of analyzed atoms per unit length: 360 atoms/nm, or the average block length. It should be kept in mind that the analyzed volume is not an ideal cylinder rather a truncated cone, since a constant tip to probe aperture distance (3 cm) is used in the analysis. Therefore, for a given block size, the block length is larger in the beginning of the analysis and smaller in the end of the analysis. However, the difference in the block length between just a few adjacent blocks is very small. In the present case a local concentration variation is in consideration, the average block length can be used.

The concentration profiles were constructed using a block size of 300 atoms, i.e., a block length of 0.8 nm. In contrast to the previous analysis, the boundary in the $YBa_2Cu_3O_{6.6}$ specimen showed a depletion of oxygen at the twin boundary. The oxygen content at the boundary region decreased by about 5–6 at. %. In the same region, the copper, barium, and yttrium contents were slightly higher than the average values. This is mostly due to the balance of oxygen depletion. The variation in oxygen concentration across the boundary region was slightly asymmetric. Concentration profiles of Y, Ba, Cu, and O are shown in Fig. 7. Besides the change in oxygen concentration at the boundary region, the width of the region is an equally important piece of information, as long as the coherence length is concerned. For the analysis across a thin plate precipitate inclined to the cylinder of analysis in a general context, the concentration profile was qualitatively presented and discussed previously (see, for example, Ref. 14, p. 203). The profile is reproduced as the lower panel of Fig. 8, where C_m and C_b denote the concentration of matrix and the plate, respectively. For the particular purpose of obtaining the width of the oxygen-depletion region in the present work, it is discovered that the thickness of the plate can be calculated from the information contained in the concentration profile. Given the measured width of C_b in the profile, denoted by W_{cb}, let W_{tb} be the width of the depletion region in the material, d_{ap} be the diameter of the cylinder of analysis, and ϕ the inclination angle. The geometric relation between these variables can be established from the upper panel of Fig. 8. W_{tb} can thus be obtained:

$$W_{tb}=W_{cb}\cos\phi+d_{ap}\ \sin\phi.$$

In this particular analysis, the average diameter of aperture was 8 nm. The inclination angle was 20°. W_{cb} can be determined as 3 or 4 nm from Fig. 7(d). The corresponding W_{tb} values are 6 or 7 nm as calculated from the above formula.

IV. DISCUSSION

The mechanism of the *T-O* transition has been identified as nucleation-and-growth mechanism,[22,23] in which the orthorhombic phase nucleates predominantly along grain boundaries, and grows into the tetragonal matrix. The growth rate is controlled by diffusion of oxygen. Based on this mechanism of the twin formation, an oxygen-depleted twin boundary model was constructed by Jou and Washburn.[24] The model gives a rather detailed account of twin boundary width, overall oxygen stoichiometry of samples, average twin domain width, and lattice parameters on the basal plane. The model assumed a perfect stoichiometric $YBa_2Cu_3O_7$ within the twin domains and $YBa_2Cu_3O_6$ at the twin boundaries. The oxygen-depleted twin boundary width can then be expressed as $W_{tb}=2jab/(a^2+b^2)^{1/2}$ (referring to Fig. 4 in Ref. 24), where j is the number of oxygen-depleted planes, and a, b are the lattice parameters on the basal plane of $YBa_2Cu_3O_7$. For a material with an average oxygen content x, the relation between the x, average twin domain width and the twin boundary width is

$$x=x(j)=6+\frac{W_t-W_{tb}(j)}{W_t}.$$

The twin domain width W_t can be calculated by $W_1 \approx ab/(b-a)$.[25]

Using this model, we can calculate the width of oxygen depletion at twin boundaries of $YBa_2Cu_3O_{6.6}$ material. Taking $a=0.382\ 27$ nm, $b=0.3891$ nm from the work of Jorgensen *et al.*,[17] the calculated twin domain width is 21.5 nm and the width of oxygen depletion region is 8.5 nm. These values give $j=16$. In the present work, the twin domain size

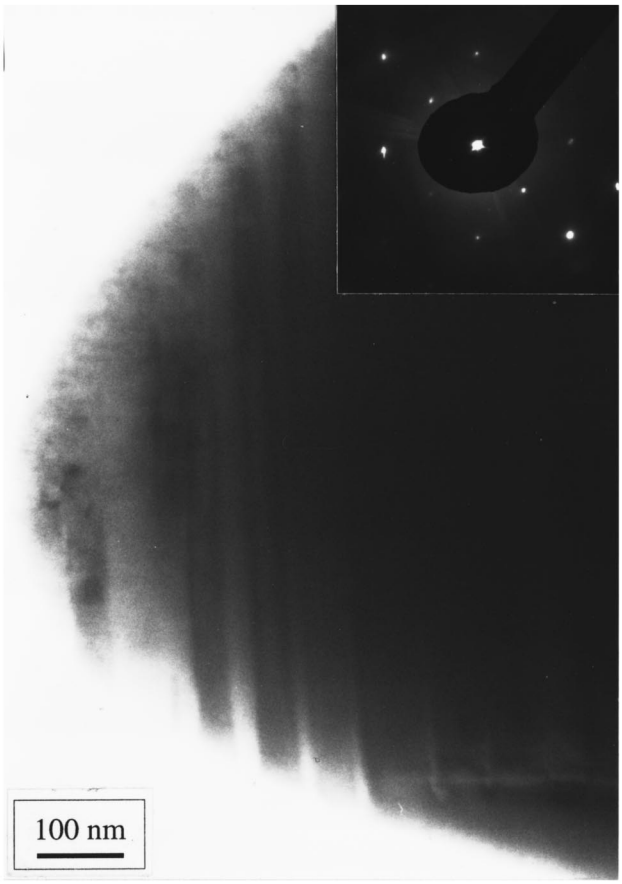

FIG. 5. TEM micrograph and selected area electron-diffraction pattern of the same tip as shown in Fig. 4.

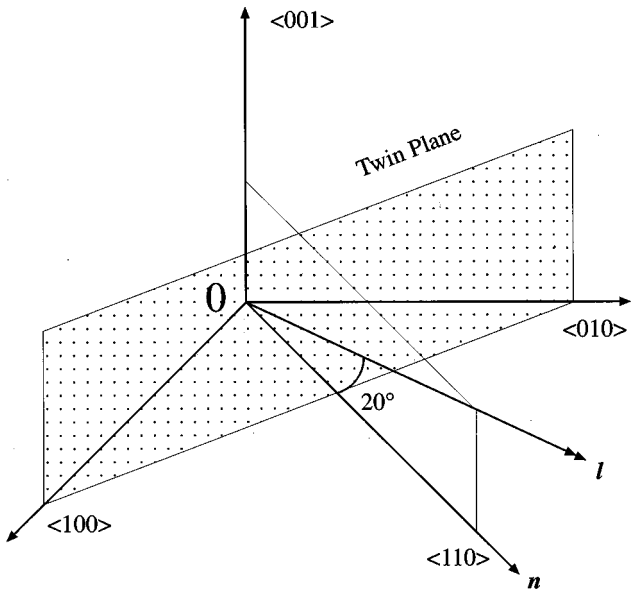

FIG. 6. Orientation relation of the direction of analysis and the twin plane, n, normal to the boundary plane, and l, direction of analysis.

is 22 nm as measured from TEM, and the width of the oxygen-depletion region is about 6–7 nm from atom-probe analysis. Evidently, the measured values agree well with the values calculated from the model.

It has been, in fact, reported that twin boundaries are not monatomic planes, rather transitional regions extending up to about 4 nm, depending on cation substitution, level of oxygenation, and heat treatment. These values were obtained from high-resolution transmission electron microscopy (HREM) observations.[26,27] However, the width of the twin boundary region obtained from HREM is essentially the width of image distortion region at the boundary. This distortion reflects the change of electrostatic potential across the twin boundary, which scatters incident electrons. The contribution to this potential is mainly from the heavy Y and Ba atoms. Therefore, the contrast of distortion is not sensitive to oxygen. To correlate the width of image distortion to oxygen depletion other factors have to be considered. Therefore the twin boundary width determined from HREM should not be expected directly comparable to the width of oxygen depletion measured by APFIM, nor the width predicted by Jou and Washburn's model.

From the comparison of the twin boundary width obtained by HREM and by APFIM it is clear that the boundary width has different physical meanings depending on the way it is measured. For the purpose of correlating twin boundary structure to superconducting properties, the width of oxygen depletion seems to be a good parameter. Nevertheless, in order to obtain complete information about twin boundary structure, one should investigate the same boundary using both HREM and APFIM techniques.

It is easy to visualize that there are two variants of {110} planes along each [110] direction in $YBa_2Cu_3O_{6+\delta}$, one consisting of oxygen atoms and oxygen vacancies, which can be referred to as the OV plane, and the other consisting of Y, Ba, Cu, and O atoms, which can be referred to as the cation plane. Due to the requirement of mirror symmetry imposed on a pair of twins with the twin boundary as the mirror plane and the fact that {110} planes are indeed twinning planes, it is natural to expect that there should be two types of twin boundaries, the OV boundaries (twin boundaries with the OV plane as the boundary plane), and the cation boundaries (twin boundaries with the cation plane as the boundary plane). These two types of twin boundaries have been observed by means of HREM.[10,28] Important observations were that the OV boundaries were found only in fully oxygenated samples, and the cation boundaries were found only in oxygen-deficient samples.[10] These observations indicate an apparent correlation between the boundary type and oxygen stoichiometry of the sample. They possibly imply that the T-O transition occurring in an oxygen-rich atmosphere tends to produce OV boundaries, whereas the transition occurring in an oxygen-depleted atmosphere tends to produce cation boundaries. However, a single boundary of mixed OV and cation types has also been observed in a fully oxygenated sample. The two parts of the twin boundary kinked at a twin boundary dislocation.[29] This observation provided a fingerprint of a possible way of twin boundary motion in T-O transformation and possible evidence of inhomogeneity in

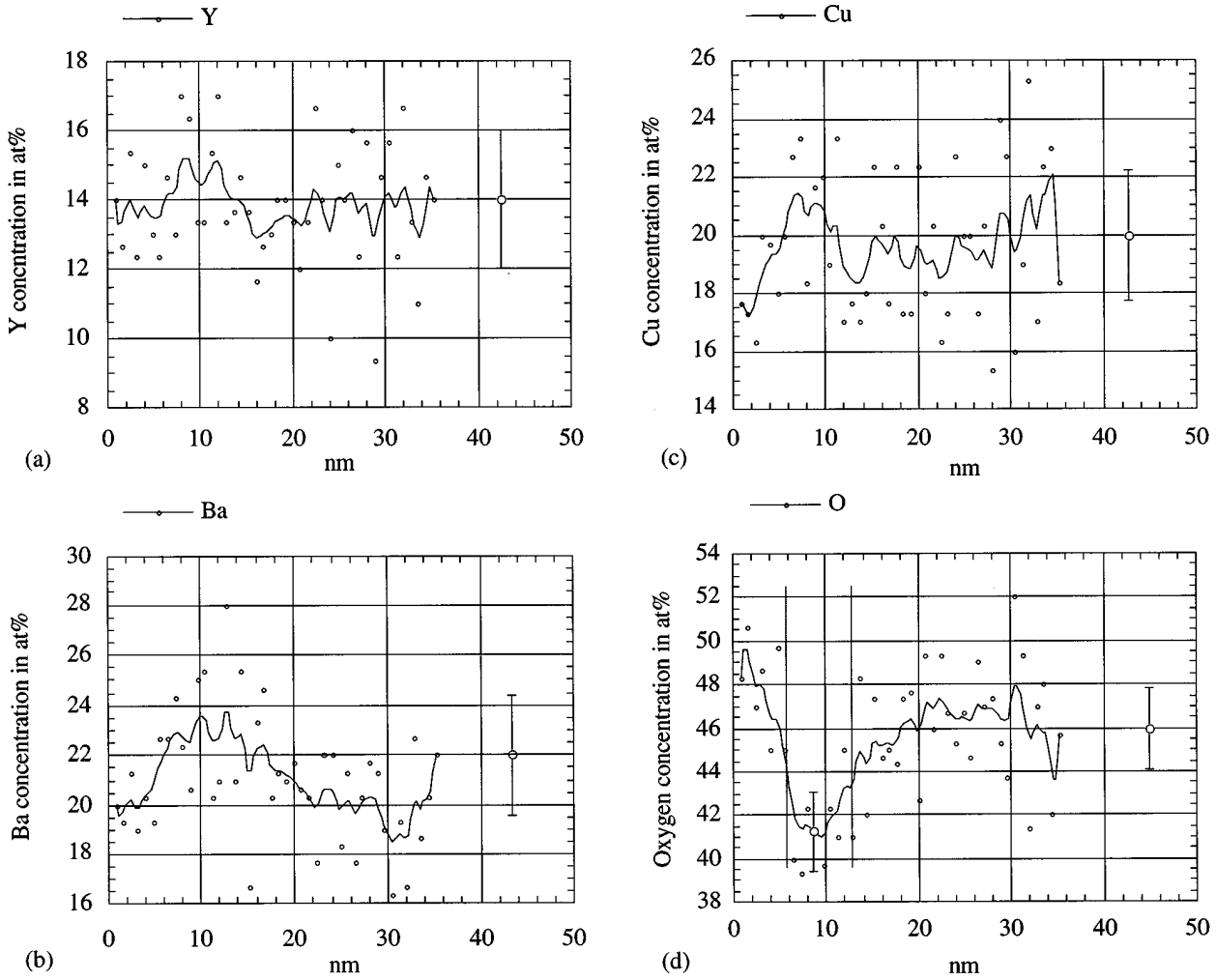

FIG. 7. Concentration profiles of Y (a), Ba (b), Cu (c), and O (d) in a $YBa_2Cu_3O_{6.6}$ specimen. The curves are the smoothened curves (running mean over 3 blocks). Circles are measured data points. Error bars represent values of 2σ. The region of oxygen depletion at the twin boundary is marked in (d).

oxygen content. It also marked the two possible direction of the dislocation motion in a subsequent heat treatment, towards cation boundary in oxygen-rich atmosphere or towards the OV boundary in a reducing atmosphere. Based on the observations concerning the OV and the cation twin boundaries, it is reasonable to conclude that the measured twin boundary in $YBa_2Cu_3O_{6.6}$ is a cation boundary. This can be further confirmed by first imaging the outmost twin boundary in a $YBa_2Cu_3O_{6+\delta}$ tip by HREM and subsequently analyzing it by APFIM.

By combining HREM and APFIM in this way it would be possible to investigate which type of boundaries is energetically favorable under certain processing conditions. We believe that results from such studies will provide valuable knowledge on the *T-O* transition and twin boundary structure in $YBa_2Cu_3O_{6+\delta}$. It would also be possible to tailor the twin boundary structure by controlling level of oxygenation, cation substitution, heat treatment, and impurity segregation in order to obtain desired electrical properties of twin boundaries for the purpose of making superconducting electronic devices, like what has been done with grain boundaries.[30] The narrow ΔT_c, from 0.2 to 2 K,[4,5] and broad resistive transition in applied magnetic field in single crystals[4] indi-

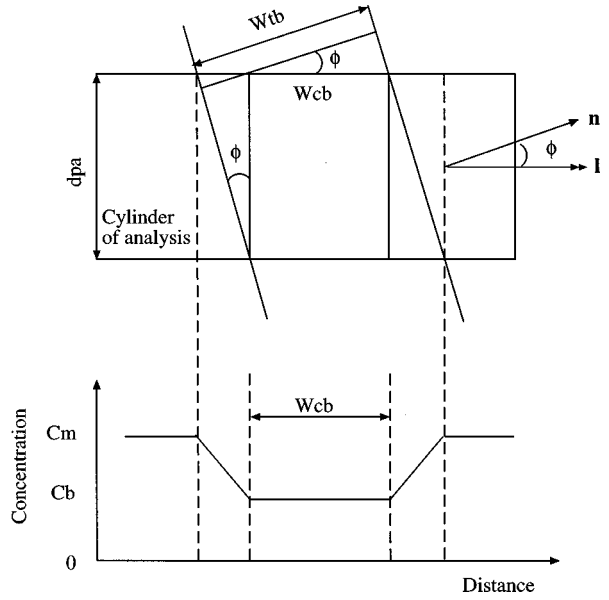

FIG. 8. The upper panel: schematic diagram of an atom probe analysis across an inclined thin plate precipitate; n, normal to the boundary plane; l, direction of analysis; ϕ, angle of inclination; and d_{ap}, diameter of the cylinder of analysis. The lower panel: corresponding schematic diagram of concentration profile.

cated that twin boundaries may act as Josephson junctions.[31] These therefore indicate the possibility of making very high-density devices based on twin boundaries.

V. CONCLUSION

APFIM of twin boundaries in $YBa_2Cu_3O_{6+\delta}$ was performed. Oxygen depletion with the spatial extension of about 6–7 nm was found at a twin boundary in the material of $YBa_2Cu_3O_{6.6}$. No depletion or enrichment was found in $YBa_2Cu_3O_{6.9}$ material. This study provided direct evidence of oxygen depletion at twin boundaries in polycrystalline $YBa_2Cu_3O_{6+\delta}$ ceramics.

ACKNOWLEDGMENTS

Financial support from TFR and the Swedish Consortium of Superconductivity is gratefully acknowledged.

[1] A. A. Abrikosov, A. I. Buzdin, M. L. Kulic, and D. A. Kuptsov, Supercond. Sci. Technol. **1**, 260 (1989).
[2] G. Deutscher and K. A. Müller, Phys. Rev. Lett. **59**, 1745 (1987).
[3] G. W. Crabtree, J. Z. Liu, A. Umezawa, W. K. Kwok, C. H. Sowers, S. K. Malik, B. W. Veal, D. J. Lam, M. B. Brodsky, and J. W. Downey, Phys. Rev. B **36**, 4021 (1987).
[4] W. K. Kwok, U. Welp, G. W. Crabtree, K. G. Vandervoort, R. Hulscher, and J. Z. Liu, Phys. Rev. Lett. **64**, 966 (1990).
[5] J. Z. Liu, Y. X. Jia, R. N. Shelton, and M. J. Fluss, Phys. Rev. Lett. **66**, 1354 (1991).
[6] V. K. Vlasko-Vlasov, L. A. Dorosinskii, A. A. Polyanskii, V. I. Nikitenko, U. Welp, B. W. Veal, and G. W. Crabtree, Phys. Rev. Lett. **72**, 3246 (1994).
[7] M. Oussena, P. A. J. de Groot, and S. J. Porter, Phys. Rev. B **51**, 1389 (1995).
[8] A. Umezawa, G. W. Crabtree, J. Z. Liu, T. J. Moran, S. K. Malik, L. H. Zunez, W. L. Kwok, and C. H. Sowers, Phys. Rev. B **38**, 2843 (1988).
[9] B. Oh, K. Char, A. D. Kent, M. Naito, M. R. Beaseley, T. H. Geballe, R. H. Hammond, and A. Kapitulnik, Phys. Rev. B **37**, 7861 (1988).
[10] Y. Zhu, in *High-Temperature Superconducting Materials Science and Engineering New Concepts and Technology*, edited by Shi D (Pergamon, New York, 1995), Chap. 5 (and the references therein).
[11] G. A. Mesyates, N. N. Syutkin, V. A. Ivchenko, and E. F. Talantsev, J. Phys. (Paris), Colloq. **49**, C6-477 (1988).
[12] A. J. Melmed, P. P. Camus, J. Vargas, and D. C. Larbalestier, Appl. Surf. Sci. **67**, 413 (1993).
[13] G. P. E. M. van Bakel, P. A. Hof, J. P. M. van Engelen, P. M. Bronsveld, and J. Th. M. de Hosson, Phys. Rev. B **41**, 9502 (1990).
[14] M. K. Miller and G. D. W. Smith, *Atom Probe Microanalysis: Principles and applications to materials problems* (MRS, Pittsburgh, 1989).
[15] M. K. Miller, A. Cerezo, M. G. Hetherington, and G. D. W. Smith, *Atom Probe Field Ion Microscopy* (Clarendon Press, Oxford, 1996).
[16] Q.-H. Hu, K. Stiller, E. Olsson, H.-O. Andrén, P. Berastegui, and L.-G. Johansson, Physica C **235-240**, 431 (1994).
[17] J. D. Jorgensen, B. W. Veal, A. P. Paulikas, L. J. Nowicki, G. W. Crabtree, H. Claus, and W. K. Kwok, Phys. Rev. B **41**, 1863 (1990).
[18] Q.-H. Hu and J. A. Alarco, Surf. Sci. **266**, 538 (1992).
[19] H.-O. Andrén, J. Phys. (Paris), Colloq. **47**, C7-483 (1986).
[20] U. Rolander and H.-O. Andrén, Surf. Sci. **246**, 390 (1991).
[21] Q.-H. Hu, K. Stiller, and H.-O. Andrén, Appl. Surf. Sci. **67**, 419 (1993).
[22] D. Shi, D. W. Capone II, K. C. Goretta, K. Zhang, and G. T. Goudey, J. Appl. Phys. **63**, 5411 (1988).
[23] D. Shi, D. W. K. Zhang, and Capone II, J. Appl. Phys. **64**, 1995 (1988).
[24] C. J. Jou and J. Washburn, J. Mater. Res. **4**, 795 (1989).
[25] C. S. Pande, A. K. Singh, L. Toth, D. U. Gubser, and S. Wolf, Phys. Rev. B **36**, 5669 (1987).
[26] Y. Hirotsu, Y. Nakamura, Y. Murata, S. Nagakura, T. Nishihara, and M. Takata, Jpn. J. Appl. Phys., Part 2 **26**, L1168 (1987).
[27] Y. Zhu and M. Suenaga, in *Interfaces in High-T_c Superconducting Systems*, edited by S. Shinde and D. Rudman (Springer-Verlag, New York, 1994), Chap. 5.
[28] Y. Zhu, M. Suenaga, J. Tafto, and D. O. Welch, Phys. Rev. B **44**, 2871 (1991).
[29] Y. Zhu and M. Suenaga, Philos. Mag. A **66**, 457 (1992).
[30] J. Alarco, Yu. Boikov, G. Brorsson, T. Caeson, G. Daalmans, J. Edstam, Z. Ivanov, V. K. Kaplunenko, P.-Å. Nilsson, E. Olsson, H. K. Olsson, J. Ramos, E. Stepantsov, A. Tzalenchuk, D. Winkler, and Y.-M. Zhang, in *Materials and Crystallographic Aspects of HT_c-Superconductivity*, edited by E. Kaldis (Kluwer Academic Publishers, Dordrecht, 1994), p. 471.
[31] M. Tinkham, Phys. Rev. Lett. **61**, 1658 (1988).